Applied Catalysis B: Environmental 162 (2015) 300–309

Contents lists available at ScienceDirect

Applied Catalysis B: Environmental

journal homepage: www.elsevier.com/locate/apcatb

Hierarchically nanostructured porous group V_b metal oxides from alkoxide precursors and their role in the catalytic remediation of VOCs

Joanna C. Rooke[a,*,1], Tarek Barakat[b,1], Julien Brunet[b], Yu Li[c], Manuel Franco Finol[d], Jean-François Lamonier[d], Jean-Marc Giraudon[d], Renaud Cousin[b], Stéphane Siffert[b,*], Bao Lian Su[a,c,*]

[a] Laboratory of Inorganic Materials Chemistry (CMI), University of Namur, 61 rue de Bruxelles, B5000 Namur, Belgium
[b] Unité de Chimie Environnementale et Interactions sur le Vivant (UCEIV), Université Lille Nord de France, Université du Littoral-Côte d'Opale (ULCO), E.A. 4492, F-59140 Dunkerque, France
[c] State Key Laboratory of Advanced Technology for Materials Synthesis and Processing, Wuhan University of Technology, 122 Hongshan Luoshi Road, 430070 Wuhan, China
[d] Unité de Catalyse et Chimie du Solide, UMR CNRS 8181, Université Lille1 Sciences et Technologies, 59655 Villeneuve d'Ascq, France

ARTICLE INFO

Article history:
Received 23 January 2014
Received in revised form 26 June 2014
Accepted 30 June 2014
Available online 8 July 2014

Keywords:
Hierarchical porosity
Group V_b metal oxides
Alkoxide chemistry
Heterogeneous catalysis
Volatile organic compounds

ABSTRACT

This study reveals how the textural properties of hierarchically porous group V_b metal oxides, prepared via a spontaneous auto-formation process, can strongly depend upon the pH of the reaction media, with an acidic media increasing the specific surface of Nb_2O_5 whereas a basic medium results in the highest specific surface for Ta_2O_5. Catalytic oxidation of toluene over Pd loaded hierarchically porous group V_b systems, and the supports alone, has shown that supports synthesised at pH 6 are the most active, despite having lower specific surfaces, thus implying modifications to the surface chemistry in the presence of H^+ or OH^- can affect the overall performance of the supported catalytic system.

1. Introduction

The three principle group V_b metals, vanadium, niobium and tantalum, and their compounds can be found in many diverse applications such as catalysis, electronics and metallurgy (alloys) due to their beneficial properties such as surface acidity and variable oxidation states. Vanadium oxide catalysts play an important role in heterogeneously catalysed reactions that rely on surface reduction and oxidation, viz. selective oxidation, ammoxidation and oxidative dehydrogenation of hydrocarbons [1]. Vanadium oxide catalysts have also been used in the production of sulphuric acid [2], selective reduction of NO_x with NH_3 [3] as well as in the total oxidation of benzene [4]. Many vanadium oxide catalysts are in fact deposited on the surface of an oxide support [5]. It was originally thought that support materials impart mechanical strength and increase the surface area, however the properties of the support material influence equally the activity and selectivity of supported metal oxide catalysts [6]. Thus it is judicious to select support materials which themselves have known catalytic properties.

Although vanadium takes the lion's share when it comes to catalytic applications of group V_b metals, there are also many reports of the use of niobium and to a limited extent tantalum based catalysts [7–20]. Niobium and tantalum (*V*) oxides are much more stable than their vanadium counterparts and subsequently much more difficult to reduce. Niobium compounds have been used in catalysis as an active phase or promoter, solid acid catalyst, support or as a redox material [7]. Niobia is an archetypal strong metal support interaction (SMSI) oxide and has been widely studied as a support for metals such as Pt, Rh, Ru, amongst others [8]. It has been found that with the use of niobia supports or niobium promoted oxide supports, the catalytic properties of the metal-support systems are enhanced whilst high selectivity is maintained. The redox potential of niobia could also improve the redox properties of these supported metals.

* Corresponding authors at: University of Namur, Laboratory of Inorganic Materials Chemistry (CMI), 61 rue de Bruxelles, B-5000 Namur, Belgium.
Tel.: +32 81 724531; fax: +32 81 725414.
E-mail addresses: joanna.rooke@unamur.be, jc_rooke@hotmail.com (J.C. Rooke), stephane.siffert@univ-littoral.fr (S. Siffert), bao-lian.su@unamur.be (B.L. Su).
[1] These authors contributed equally to this work.

http://dx.doi.org/10.1016/j.apcatb.2014.06.056
0926-3373/

Both niobium and tantalum oxides are acidic, especially when amorphous, although this acidity decreases upon increasing temperature [9]. The hydrated form of Nb_2O_5 was found to be active in the gas phase hydration of ethane to form ethanol [10]. Nb_2O_5 has also proven to be an efficient catalyst in the transesterification of β-keto esters with several types of alcohol [11]. Niobia catalysts have found use in pollution abatement as well, such as the selective catalytic reduction (SCR) of NO_x by NH_3. The addition of Nb_2O_5 to a well known catalyst for this process (V_2O_5–TiO_2) improved the low temperature activity of the catalytic system [12]. Ta_2O_5 has also been investigated for its catalytic properties, such as the activation of propane and butane [13] or when supported on a secondary metal oxide support [14]. Using the methanol oxidation reaction Chen et al. revealed how the choice of supporting oxide influenced reactivity and selectivity of the surface TaO_x species, dependent on the bridging Ta—O— support bond, with silica supports creating redox characteristics where as alumina, titania and zirconia yielded surface acidity.

Material morphology plays a big role in the activity of a catalyst. Aerogels and xerogels of niobia were compared against commercial products in the cracking of *n*-heptane [15]. During sintering, the BET surface areas were reduced in all three materials but this was more pronounced in the commercial niobia. The aerogels also possessed less labile hydroxyls and more acidic sites than the commercial product. As a result, cataytic results were much higher for the aerogels than for the commercial products. Nakajima et al. synthesised mesoporous $Nb_2O_5{\cdot}nH_2O$ and compared its catalytic activity to that of supermicroporous and bulk $Nb_2O_5{\cdot}nH_2O$ in the hydrolysis of cellobiose and Friedel–Crafts alkylation (FCA), where they found that mesoporous hydrated niobia was advantageous for hydrophilic but not hydrophobic FCA reactions [16]. Mesoporous Ta_2O_5 has been employed in the photocatalytic decomposition of water by Takahara et al. [17] and for photocatalytic H_2 evolution by Sreethawong et al. [18]. In both cases photocatalytic activity increased with cocatalyst loading using NiO.

Interest in the textural properties of group V_b metal oxides resulted in the discovery of a family of mesoporous Nb_2O_5 [19] and Ta_2O_5 [20] molecular sieves by Antonelli in 1996, via the use of a novel ligand assisted templating strategy. Leading on from this it has been shown that hierarchically porous Nb_2O_5 and Ta_2O_5 materials can be obtained through spontaneous auto-formation by simply reacting a suitable metal alkoxide in water [21]. The hydrolysis and polycondensation of a metal alkoxide or $Al(CH_3)_3$ results in the release of small molecules that act as porogens in the hierarchically porous forming oxide, without the need for a templating agent [22]. Micellar solutions can however also be used as to boost the specific surface areas obtained [23]. Titania and zirconia materials prepared in this way have found to be excellent supports for noble metals when used in the total catalytic oxidation of VOCs [24]. The selectivity of a catalyst is often dependent on the geometry and size of the pores, with micro and mesopores improving the catalyst's selectivity. However such small pores often suffer from diffusion limitations, hence it is of interest to introduce macroporosity into (micro) mesoporous systems to help with matter transfer. This can be achieved through the spontaneous auto-formation procedure described above. Hierarchical porosity is a key factor in the increase in accessibility within a material, as the macropores are interlinked with the (micro) mesoporous networks and can thus funnel reactants towards the active sites of the catalyst, located within a more confined space [25]. By varying the parameters of this process one can obtain a wide range of morphologies. Studies have shown how a careful control of the water present during the hydrolysis of metal alkoxides can directly influence the porosity and surface area of the resultant oxide [26].

In this work the effect of pH and the presence of a non-ionic surfactant in the reaction media on product morphology have been studied in the synthesis of hierarchically porous group V_b metal oxides. The materials obtained were examined in terms of catalytic activity in the total oxidation of toluene and compared to benchmark hierarchically porous titania catalysts prepared in a similar fashion to evaluate their suitability as active supports for noble metals such as Pd, as demonstrated herein. The relationship between surface chemistry relying on the synthesis conditions and the catalytic activities of Pd catalysts supported on hierarchically porous group V_b metal oxides has been discussed.

Table 1
Material preparation conditions.

Material	Precursor	Surfactant	pH[a]
A	$OV(OC_3H_7)_3$	Brij 56	2
B	$OV(OC_3H_7)_3$	Brij 56	6
C	$OV(OC_3H_7)_3$	Brij 56	12
D	$OV(OC_3H_7)_3$	–	2
E	$OV(OC_3H_7)_3$	–	6
F	$OV(OC_3H_7)_3$	–	12
G	$Nb(OEt)_5$	Brij 56	2
H	$Nb(OEt)_5$	Brij 56	6
I	$Nb(OEt)_5$	Brij 56	12
J	$Nb(OEt)_5$	–	2
K	$Nb(OEt)_5$	–	6
L	$Nb(OEt)_5$	–	12
M	$Ta(OEt)_5$	Brij 56	2
N	$Ta(OEt)_5$	Brij 56	6
O	$Ta(OEt)_5$	Brij 56	12
P	$Ta(OEt)_5$	–	2
Q	$Ta(OEt)_5$	–	6
R	$Ta(OEt)_5$	–	12

[a] pH 2 H_2SO_4, ca. pH 6 Milli-Q H_2O and pH 12 NH_4OH.

2. Experimental

2.1. Synthesis of group V_b metal oxides from alkoxide precursors

Vanadium, niobium and tantalum oxide materials were fabricated by exploiting the reactivity of group V_b metal alkoxides in aqueous solutions. It has previously been reported that hierarchically porous materials can be obtained via an auto-formation process using metal alkoxides [21–24,26], and the textural and morphological properties of these materials can be improved by a careful engineering of the reaction conditions. In this work, two factors were taken into consideration, the use of a neutral surfactant and the pH of the reaction medium. A series of materials (Table 1) were prepared in the presence of a micellar solution of 10 wt% Brij 56 (Aldrich), a neutral surfactant, at 3 different pH values: pH 2 (H_2SO_4), ca. pH 6 (Milli-Q H_2O) and pH 12 (NH_4OH). The micellar solutions were prepared by heating the surfactant to 60 °C in pH adjusted Milli-Q water, as defined above, until dissolved then maintaining the solution at 60 °C under gentle agitation (<150 rpm) for several hours. The solution was then decanted into a shallow dish to increase the accessible surface area and the alkoxide precursor, either $OV(OC_3H_7)_3$ (2.7 g, Aldrich, 98%), $Nb(OEt)_5$ (2.5 g, Aldrich, 99.95%) or $Ta(OEt)_5$ (2 g, Aldrich, 99.98%) was added dropwise to this micellar solution. After ca. 10 min the solution and the oxide precipitate was transferred to a Teflon lined autoclave and subjected to a hydrothermal treatment at 80 °C for 24 h. After cooling the surfactant was extracted with ethanol using the Soxhlet technique for ca. 72 h and the product was recuperated and dried at 60 °C overnight.

Conversely a second series of materials (Table 1) was simply synthesised via the dropwise addition of the same quantity of the respective alkoxide precursor, $OV(OC_3H_7)_3$, $Nb(OEt)_5$ or $Ta(OEt)_5$, into a shallow dish containing 50 mL pH adjusted water [pH 2 (H_2SO_4), pH 6 (Milli-Q H_2O), pH 12 (NH_4OH)], under gentle agitation at room temperature (i.e. in the absence of the Brij 56

surfactant). After the reaction had taken place the material was recuperated through filtration and dried at 60 °C overnight prior to characterisation, no hydrothermal treatment was undertaken.

2.2. Elaboration of palladium catalysts

The as-synthesised Nb_2O_5 and Ta_2O_5 were used as catalytic supports for palladium nanoparticles. The supports were first calcined at 400 °C for 4 h with a ramp rate of 1° min^{-1} prior to catalyst preparation. The catalytic systems were prepared using the aqueous impregnation method. A pre-determined amount of $Pd(NO_3)_2$ solution (Alfa Aesar, 99.9%) was mixed with the support for 30 min, such that the target impregnation was 0.5 wt% Pd. The water was then removed by rotovaporation and the material calcined under air (2 L h^{-1}) at 400 °C for 4 h with a ramp rate of 1° min^{-1}. Prior to catalytic testing a known quantity of impregnated material was reduced under flowing 5% hydrogen (2 L h^{-1}) mixed with Argon at 200 °C for 2 h.

2.3. Catalytic testing

The complete oxidation of a test pollutant, toluene, over 100 mg of each catalytic system described above was carried out in a conventional fixed bed reactor with a temperature rise of 1 °C min^{-1}. The flow of toluene was set at 1000 ppm in a flow of air: (total flow of 100 mL min^{-1}). The products formed during combustion were analysed and quantified via gas chromatography using a CP-4900 microGC (Varian) with injections taken every 3 min. From these measurements conversion graphs were constructed to determine the temperature at which a 50% conversion had taken place, which was then compared to a series of previously published hierarchically porous TiO_2–ZrO_2 catalyst supports [27] and also commercial oxides of Nb_2O_5 and Ta_2O_5 in the presence and absence of Pd.

2.4. NH_3 temperature programmed desorption

The density of acid sites in the samples was determined by temperature programmed desorption of ammonia (NH_3-TPD) using a Micrometrics AUTOCHEM 2920 apparatus equipped with a mass spectrometer. Around 100 mg of sample were purged for 30 min in a He flow of 30 mL min^{-1} at 300 °C before being cooled to 80 °C. The sample was then placed in contacted with a 10% NH_3/He atmosphere for 30 min in a 30 mL min^{-1} flow before being further purged for 2 h at 80 °C under a 50 mL min^{-1} He flow. After purging, the temperature was raised at a rate of 10 °C min^{-1} to 700 °C in a 30 mL min^{-1} He flow. The quantity of desorbed NH_3 was determined by mass spectrometry using the peak with $M/Z = 15$.

2.5. Material characterisation techniques

Textural properties of the materials were analysed via adsorption–desorption of nitrogen at -196 °C using a Micromeritics Tristar 3000 porosimeter with prior outgassing to $\sim 10^{-4}$ bar, small angle powder X-ray diffraction (PXD) using a PANalytical X'pert PRO diffractometer (supporting information) and scanning electron microscopy (SEM) using a Hitachi S-4800 microscope.

3. Results and discussion

The reaction between each group V_b alkoxide precursor and an aqueous solution, independent of pH and the use of surfactant, was instantaneously visible. However the materials obtained varied greatly, as detailed below.

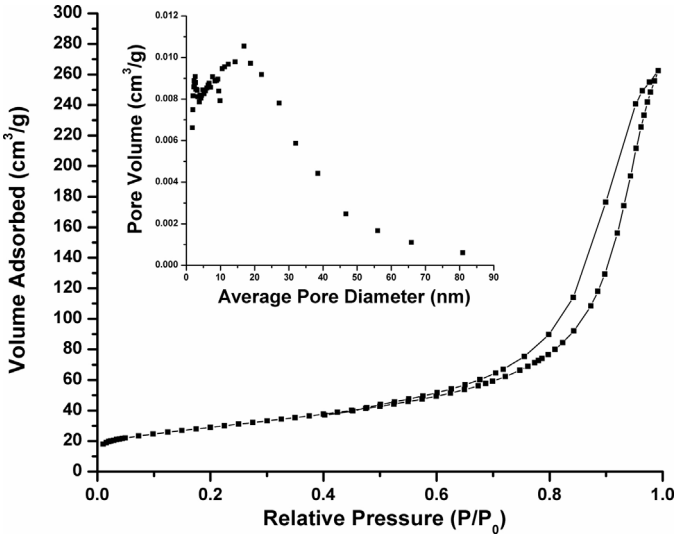

Fig. 1. N_2 adsorption–desorption isotherm and (inset) corresponding pore size distribution of material C.

3.1. Vanadium oxide

Upon addition of vanadium oxytripropoxide to a pH 2 or 6 media without surfactant, the aqueous solution turned a vivid yellow colour, with a red–orange film on the surface, indicative of V^{5+} (colouration due to a charge transfer process). V_2O_5 itself is soluble in both acidic and alkaline solutions which limits the formation of hierarchically structured vanadium oxide materials. The film broke up into flake like particles and fell to the bottom. After recuperation of the product and drying, the final powders were blue–black in colour owing to reductive processes, with the colour of VO_2 being blue–black, which is insoluble in water [28]. The material aggregated together forming a hard lump which was difficult to grind. There was also a small amount of reflective particles indicative of the formation of vanadium metal. When the process was carried out at pH 12, the precursor formed orange droplets but this colour faded after a few minutes. The final materials ranged from light yellow-brown to dark brown; in such cases a grindable powder was obtained. Similar results were obtained when using a surfactant, where a brown powder is obtained at pH 12 but at all other pH the material is blue–black (cf. VO_2).

Only material C was found to be porous with a $S_{BET} = 104\ m^2\ g^{-1}$ and $V_{BJH} = 0.38\ cm^3\ g^{-1}$. The isotherm given in Fig. 1 is indicative of a material that is an aggregate of nanoparticles with an H3 hysteresis loop which tends to result from 'aggregates of platy particles or adsorbents containing slit-shaped pores' [29]. The pore size distribution is centred around 16 nm suggesting a degree of mesoporosity within material C.

From SEM studies in Fig. 2 it was seen that for materials that had undergone ethanolic extraction of the surfactant, the material surface appeared as if it were rippled and at high magnification a rod-like morphology over the material surface was visible (Fig. 2b, d and f). For those materials made without surfactant no overall uniform morphology was found. For instance only in material D (pH 2) is there clear evidence of macropores (Fig. 2g and h), similar to those seen in previous studies using other metal alkoxides where an oxide crust forms over the surface and underneath a more textured material forms owing to the liberation of small porogen type molecules [22]. At pH 6 (E) the material (Fig. 2i and j), has a similar rippled effect as seen in the materials fabricated with surfactant. Although in this case at higher magnification there are no rod like structures, just what appears to be the edges of layered sheets (Fig. 2j). At pH 12 (F) there are smooth baton like particles that form

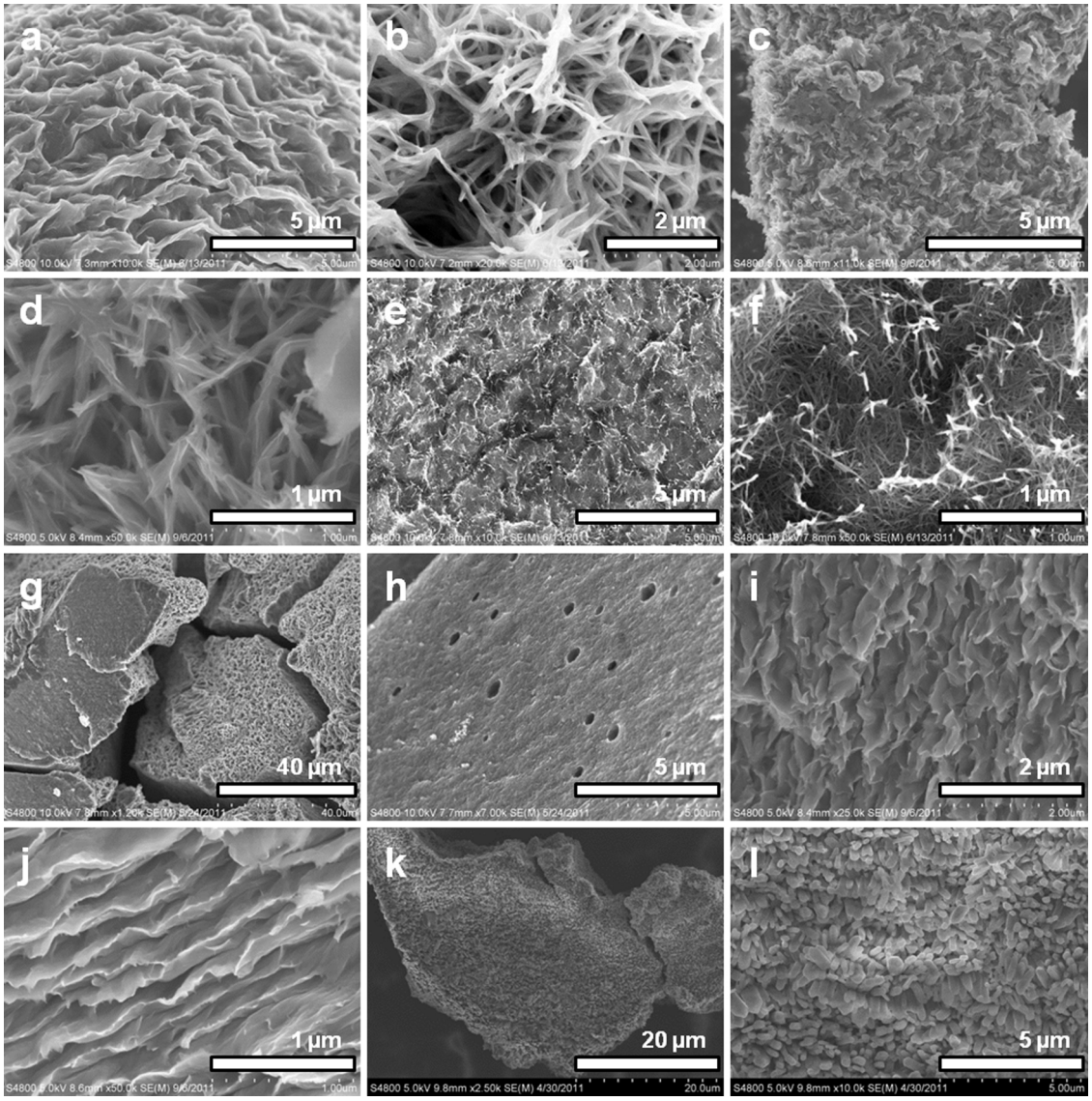

Fig. 2. Scanning electron microscopy images for the various vanadium oxides, where (a) and (b) correspond to material A, (c) and (d) to B, (e) and (f) to C, (g) and (h) to D, (i) and (j) to E and (k) and (l) to material F.

during the reaction of alkoxide in aqueous solution (Fig. 2l). These different morphologies highlight how the pH of the reaction media can vastly influence the forming product. The solubility of the vanadium oxide changes dependent on oxidation state and pH, thus the vanadium oxide recuperated is that which has formed once saturation has been reached. Hence it would be interesting to use a non-reactive medium into which a controlled amount of water is added to the system to minimise dissolution. Previous studies have shown that the morphology of porous titanium oxides prepared using alkoxides in an auto-formation technique can vary greatly dependent on the water content of the reaction system [26].

3.2. Niobium oxide

Independent of the properties of the reaction media, a white powder is formed on addition of the $Nb(OEt)_5$ precursor. The textural properties of these powders are however dependent on the pH of the reaction media as can be seen in Table 2. Interestingly the pH of the reaction media plays a significant role in the textural properties of the resultant Nb_2O_5 material. At lower pH (2 and 6) the specific surface area is substantially larger than in alkaline media, irrespective of the presence of surfactant. Surfactant plays its part too by increasing the surface area and porous volume of the resultant Nb_2O_5 synthesised at the same pH as one synthesised without surfactant, cf. G vs J, H vs K and I vs L, as the micelles act as templates around which the Nb_2O_5 can form, imparting additional porosity.

Table 2
Textural properties of hierarchically porous Na_2O_5 synthesised under different reaction conditions.

Material	Conditions	S_{BET} ($m^2\ g^{-1}$)	V_{BJH} ($cm^3\ g^{-1}$)
G	pH 2, surfactant	359	0.42
H	pH 6, surfactant	355	0.33
I	pH 12, surfactant	68.8	0.07
J	pH 2	243	0.09
K	pH 6	227	0.22
L	pH 12	9.3	0.016

Nitrogen sorption results (Fig. 3) have revealed that each material has a microporosity, with the pore size distributions centred below 2 nm. The uptake at lower relative pressures is greater for materials G, H, J and K than for I and L suggesting a greater degree of

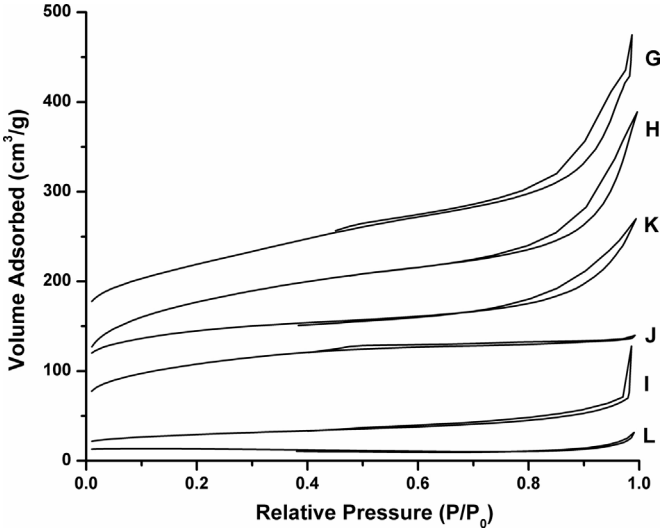

Fig. 3. Nitrogen adsorption–desorption isotherms for the various Nb_2O_5 materials where G is offset by 120, H by 80, K by 80, J by 40 I and L by 10 $cm^3\ g^{-1}$ for clarity.

microporosity in these materials, which probably accounts for their greater porous volumes as found by the BJH method. However the isotherms themselves follow approximately that of a IUPAC type II isotherm. The isotherms are typical of an aggregation of nanoparticles, and often saturation is not reached indicating a degree of macroporosity in the materials, confirmed by a strong uptake in nitrogen at high relative pressures and a late onset of the hysteresis loops. These results lend themselves to the idea of hierarchical porosity within one single material, suggesting that the macroporosity stems from the aggregation of microporous Nb_2O_5 particles.

SEM studies have shown that the porosity in the materials mainly arises from the fusion of nanoparticles. Macropores are clearly visible in many of the micrographs displayed in Fig. 4, however material G has some very large macropores in the order of 20 μm, as seen in Fig. 4b, similar to the macropores formed in hierarchically porous titania and zirconia materials [21,23,26]. At more alkaline pH, in the presence of surfactant (I), a regular array of macropores can be seen that have been covered with nanoparticles over the surface (Fig. 4d). This might explain the reduction in porosity of this material in comparison to other materials prepared using a micellar solution as the pores become blocked. The macropores that form during the spontaneous reaction of alkoxide and water are more clearly identified when no surfactant is used. When the pH is low, there is a multimodal cratering across the surface of the material (Fig. 4f) and evidence of the channels carved out by the liberated porogens (Fig. 4g). As the pH increases to that of Milli-Q the macropores are quite regularly arranged, with their walls constructed from nanoparticles that have fused together (Fig. 4h). At pH 12, again the macropores are present yet there is less evidence of the fusion of nanoparticulate matter (Fig. 4i). This is in agreement with the decrease in surface area of this material as seen in nitrogen sorption studies as it would suggest there is little mesoporosity in the sample which usually arises from the interparticulate wormlike voids between nanoparticles.

3.3. Tantalum oxide

As for $Nb(OEt)_5$, a white powder is obtained on addition of $Ta(OEt)_5$ to the reaction media irrespective of the pH, yet the

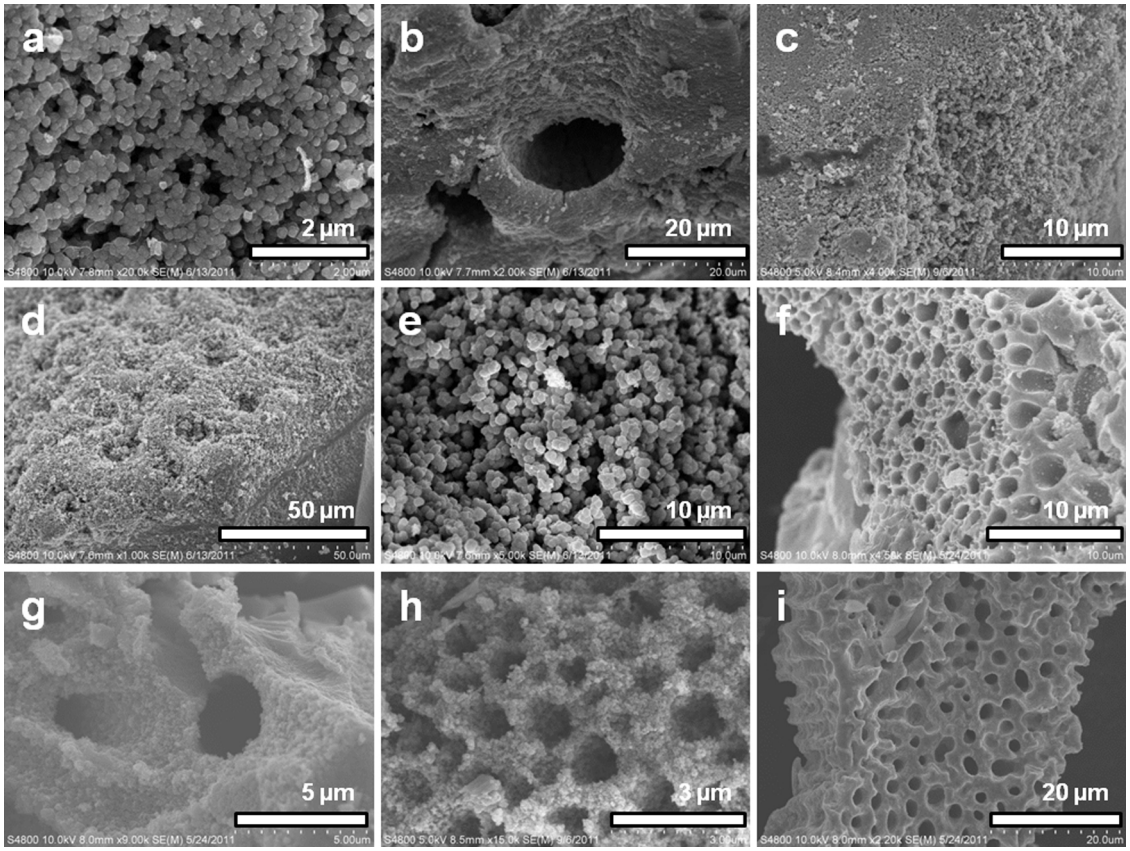

Fig. 4. Scanning electron microscopy images for the various Nb_2O_5 materials, where (a) and (b) correspond to material G, (c) to H, (d) and (e) to I, (f) and (g) to J, (h) to K and (i) to material L.

Table 3
Textural properties of hierarchically porous Ta_2O_5 synthesised under different reaction conditions.

Material	Conditions	S_{BET} ($m^2\ g^{-1}$)	V_{BJH} ($cm^3\ g^{-1}$)
M	pH 2, surfactant	100.8	0.083
N	pH 6, surfactant	159	0.09
O	pH 12, surfactant	200	0.31
P	pH 2	28.4	0.035
Q	pH 6	57	0.09
R	pH 12	146	0.2

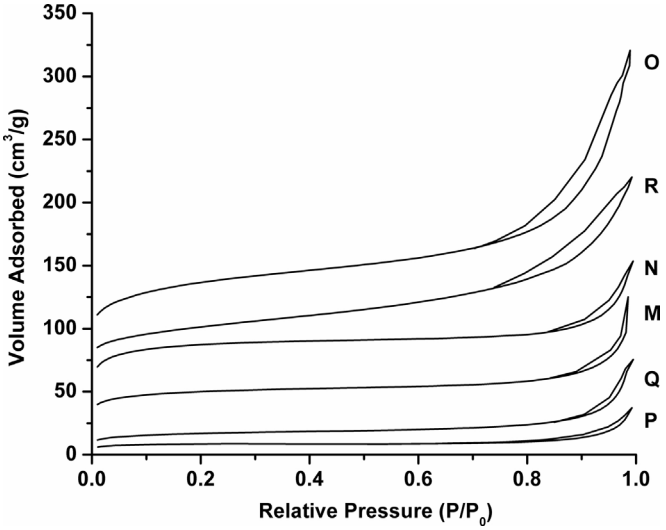

Fig. 5. Nitrogen adsorption–desorption isotherms for the various Ta_2O_5 materials where M is offset by 20, N by 40, O by 80 and R by 60 $cm^3\ g^{-1}$ for clarity.

textural properties of the resultant oxide depend greatly on the pH of the system (Table 3). In juxtapose to the as-synthesised Nb_2O_5, the surface area and mesoporous volume of the Ta_2O_5 formed decrease on decreasing pH (Table 3). Again there is an increase in surface area when using surfactant owing to the templating effect.

Again nitrogen sorption studies have revealed that the materials are micro (macro)porous with pore size distributions centred below 2 nm yet the isotherms have a late uptake of nitrogen at high relative pressures, consistent with a macroporous material (Fig. 5). The hysteresis loops, following that of H3 type loops, are consistent with slit like pores.

SEM reveals that the porosity and elevated surface areas of these Ta_2O_5 materials arises predominately from the aggregation of nanoparticles with only occasional evidence of the auto-formation of the macrochannels seen in other metal oxides obtained from alkoxides in water [21–24,26]. Considering the N_2 sorption study, where no saturation is attained at high P/P_0 thus indicating some degree of macroporosity, this porosity most likely arises from the aggregation of microporous Ta_2O_5 particles which has led to the irregular shaped openings on the surface. There are no wide scale regions of quasi aligned macrochannels as seen for niobia samples (Fig. 4) yet in places small macropores can be seen underneath the surface nanoparticles (i.e. Fig. 6f). Material P, synthesised at pH 2 without surfactant, does show some cratering on the surface of the oxide which could stem from the liberation of small porogen molecules (Fig. 6d).

The rate of hydrolysis and condensation of a metal alkoxide is influenced in part by the partial charge on the central metal atom. In turn this has an effect on the efficacy of the auto formation process. Titanium and zirconium alkoxides facilely undergo an auto formation process to form macrochannels within the resultant metal alkoxide, giving elevated surface areas and porous volumes [22,26]. This has also proved the case for $Nb(OEt)_5$ and $Ta(OEt)_5$ [22b,c], though the values attributed to surface area and porous volumes are generally lower. This could stem from a reduction in reactivity attributed to a reduction on the partial charge on the central metal atom, with $\delta+$ equal to ca. +0.63 for $Ti(OEt)_4$ and +0.65 for $Zr(OEt)_4$ but only +0.53 and +0.49 for $Nb(OEt)_5$ and $Ta(OEt)_5$, respectively, ($VO(OEt)_3$ is +0.46 for comparison) [30]. These reaction rates, alongside particle size, are also influenced by the presence of an acid or base catalyst. In acid media, hydrolysis is catalysed by the acidic protons through protonation of the alkoxy leaving groups. During polymerisation, colloids form with a positive surface charge which can hinder aggregation owing to repulsive forces. A smaller particle size may result in higher surface areas. In basic conditions the main nucleophile is the hydroxide ion, though strong nucleophiles are produced via the deprotonation of the hydroxo ligand which in turn increases the condensation rate and increases the rate of precipitation. It has been stated that in acid catalysed reactions the least positively charged species will react faster ($Ta(OEt)_5$ rather than $NbOEt)_5$) whereas in base catalysed reactions the opposite is true with the more positive species, in this case $Nb(OEt)_5$, reacting fastest [30]. The reaction time might be one factor in the formation of large surface areas, as a slower reaction could allow the creation of a more open framework with greater porosity and higher surface areas. This could then support the fact that Nb_2O_5 systems synthesised in acid media have higher surface areas than those synthesised in basic media as $Nb(OEt)_5$ reacts slower in acidic conditions than in basic conditions, according to the partial charges on the alkoxides, whereas the converse is true for Ta_2O_5 systems.

Sol–gel chemistry is thus an ideal tool to control parameters such as specific surface area, pore size distribution, and material purity which are key factors in the performance of a catalyst as they can be exploited to increase the number of active sites on a material surface whilst minimising species that might poison the surface such as counter ions found in traditional inorganic salt precursors.

3.4. Catalytic oxidation of toluene

The niobium and tantalum pentoxide materials presented herein have been tested for their activity in the catalytic destruction of a model aromatic VOC, toluene, to evaluate their suitability as active supports for noble metal nanoparticles. Similar hierarchically porous materials have been known to boost the performance of catalytic systems [24] proving that the chemical composition of a support material is an essential key to increased activity. The vanadium oxide samples however were not tested as many samples formed dense blocks which were difficult to grind. Based on the colour of the samples it was clear that VO_2 and not V_2O_5 had been formed in some cases. Although the surface morphology of these samples was interesting (Fig. 2), there was a lack of hierarchical porosity in these samples. For these reasons a fair comparison between V_2O_5 and Nb_2O_5/Ta_2O_5 synthesised under all conditions could not be made.

The data in Table 4 and S.I. 3 highlights a general trend that in the absence of noble metals the niobium oxide supports are more catalytically active than tantalum oxide supports, with even a partial oxidation of toluene (>10% conversion) over Ta_2O_5 taking place at temperatures in excess of 400 °C. In contrast it is possible at 380 °C to have a 70 to 90% conversion of toluene over Nb_2O_5 supports synthesised at pH 6. One significant factor for this may be down to the surface area of the support material. Results in Tables 2 and 3 reveal that the BET surface area of uncalcined niobium oxide is greater than its tantalum oxide analogue at neutral and acidic pH. The only synthesis conditions which yield the oxidation of toluene at lower temperatures for Ta_2O_5 cf its Nb_2O_5 analogue occur at pH 12 in the presence of surfactant (O vs I) and quasi identical conversion for the Ta and Nb supports synthesised in basic conditions (pH 12) in the

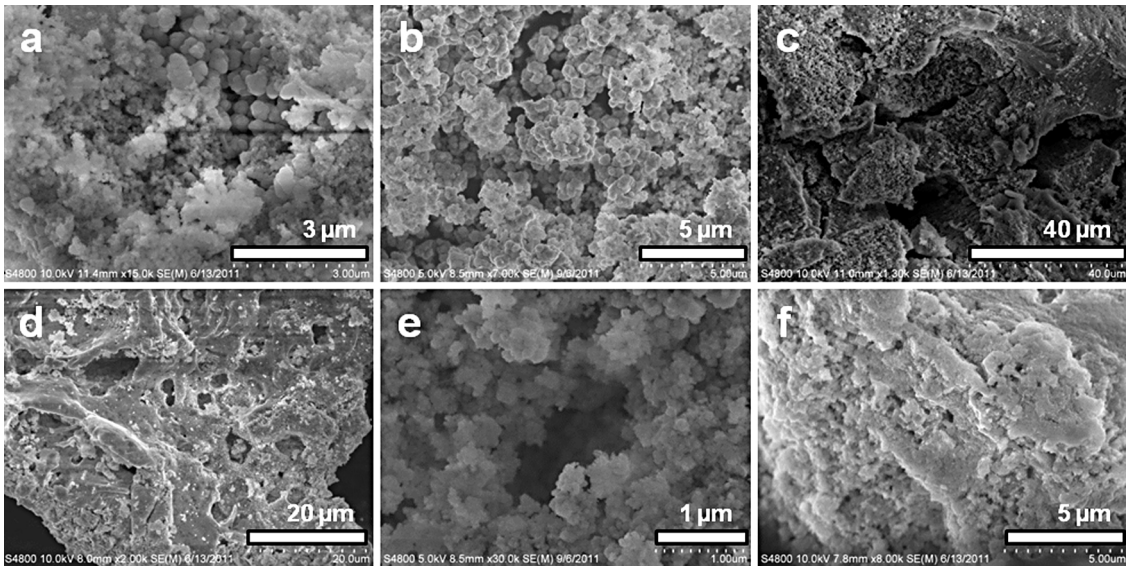

Fig. 6. Scanning electron microscopy images for the various Ta_2O_5 materials, where (a) corresponds to material M, (b) to N, (c) to O, (d) to P, (e) to Q and (f) to material R.

Table 4
Temperatures at which 30, 50 and 90% conversion of toluene is achieved for various catalytic systems.

Catalyst	Conditions[a]	T_{30} (°C)	T_{50} (°C)	T_{90} (°C)
G (Nb_2O_5)	2, *S*	372	383	400
H (Nb_2O_5)	6, *S*	353	368	400
I (Nb_2O_5)	12, *S*	>400	>400	>400
J (Nb_2O_5)	2	392	>400	>400
K (Nb_2O_5)	6	335	343	356
L (Nb_2O_5)	12	369	384	>400
M (Ta_2O_5)	2, *S*	>400	>400	>400
N (Ta_2O_5)	6, *S*	383	397	>400
O (Ta_2O_5)	12, *S*	383	>400	>400
P (Ta_2O_5)	2	>400	>400	>400
Q (Ta_2O_5)	6	390	399	>400
R (Ta_2O_5)	12	390	>400	>400

[a] Number represents pH of reaction media, *S* implies a surfactant was used during synthesis.

absence of surfactant. This also could be correlated to the increase in Ta_2O_5 BET surface area, which in fact is far superior to its Nb_2O_5 analogue in both cases (I and L).

In general it appears that the most active supports are those synthesised in distilled water alone. Nb_2O_5 has a good conversion of toluene at higher temperatures for supports synthesised at pH 6 and to some extent also for those at pH 2, with the supports synthesised without surfactant having a greater activity and better selectivity for CO_2 over CO compared to those with surfactant (H vs K and G vs J), see S.I. 3 and Table 5. This would indicate that although surface area can play a role in activity it is not necessarily so that a higher surface area will yield the greatest activities. The final acidity of the support may also be affected by the synthesis conditions and should also be taken into consideration. In comparison the Ta_2O_5 samples again showed better activity when synthesised at pH 6, however the second best activity was found in the samples synthesised under basic and not acidic conditions, which could be due to increased surface areas of pH 12 samples vs pH 2 samples although the samples with the best activity (pH 6) again did not have the largest surface areas. The use of surfactant may also pollute the surface of the oxide as incomplete removal of the template can lead to coke formation during calcinations.

In the absence of palladium one can see that the selectivities of these supports are quite low, with a high percentage of CO and benzene being formed. One important factor in the environmental remediation of VOCs is that the creation of more noxious by-products is avoided. Thus these results show that whilst the supports themselves are active, the use of noble metals such as Pd, Pt and Rh are also essential as they not only reduce the energetic costs by reducing the working temperature of the catalytic system but they also reduce the emission of toxic by-products by increasing CO_2 selectivity.

When Pd is added to the system there is much greater improvement in the tantalum systems with the $T_{50\%}$ values being ca. 10 °C lower than the corresponding niobia analogue in several cases (H vs N, K vs Q and L vs R), see Table 6 and S.I. 4. This could suggest that the interaction between Pd and Ta_2O_5 is greater than with Nb_2O_5 potentially facilitating the reduction of PdO species through an electron transfer mechanism. It is also possible that Ta_2O_5 favours the stabilisation of smaller, more active PdO nanoparticles. Though these hypotheses would require further study to determine the underlying cause.

In general the best activity is found for Pd/supports synthesised at pH 6 although low temperature activity of Pd/G (pH 2) is marginally higher which resulted in a superior CO_2 formation rate at low temperature (Table 7). These results could imply that the surface properties of the supports are influenced by the presence of H^+/OH^- species during synthesis, even after calcinations at 400 °C. Thus in optimising a catalyst system one must take into account the synthesis procedure as well as the final textural properties of a catalytic support.

There is also a noticeable difference in the temperature at which total conversion is obtained. This is in many cases lower, sometimes substantially lower, for a Pd/Ta_2O_5 system compared to its analogous Pd/Nb_2O_5 system. The $T_{100\%}$ is also lower than for Pd/TiO_2 prepared in an identical fashion from titanium isopropoxide and reported in a previous study (220 °C vs 260 °C, pH 12 no surfactant) [31], although low temperature activity remained superior for TiO_2.

Table 8 reveals catalytic data for commercial oxides in the total destruction of toluene. These samples were non-porous with low surface areas (>0.2 $m^2\,g^{-1}$). Here it can be seen that without the addition of Pd the commercial oxides have much lower conversion rates than the hierarchically porous as-synthesised supports, thus demonstrating the interest in supports with high surface area and porosity. In the presence of Pd it is observed that the light-off curves (S.I. 5) of both Nb_2O_5 and Ta_2O_5 are very similar, highlighting

Table 5
Catalytic activity and selectivity in the oxidation of toluene over hierarchically porous supports.

Catalyst	Conditions[a]	T (°C)	Toluene conversion (%)	Selectivity (%)		
				CO_2	CO	Benzene
G (Nb_2O_5)	2, *S*	300	5.4	3.1	0.0	0.03
		380	50	32	9.9	0.83
H (Nb_2O_5)	6, *S*	300	6.8	3.0	0.0	0.07
		380	75	70	4.3	0.60
I (Nb_2O_5)	12, *S*	300	0	0	0	0
		380	14	14	0.89	0.22
J (Nb_2O_5)	2	300	5.4	2.2	0.0	0.15
		380	41	26	5.0	1.0
K (Nb_2O_5)	6	300	12	4.1	0.20	0.27
		380	99.5	98	0.0	0.47
L (Nb_2O_5)	12	300	0	0	0	0
		380	27	16	3.3	1.3
M (Ta_2O_5)	2, *S*	300	1.6	1.3	0.0	0.0
		380	9.9	6.5	2.2	0.12
N (Ta_2O_5)	6, *S*	300	3.5	1.9	0.0	0.0
		380	34	26	4.9	0.49
O (Ta_2O_5)	12, *S*	300	5.6	1.8	0.0	0.0
		380	31	17	7.5	0.22
P (Ta_2O_5)	2	300	0.45	0.57	0.0	0.0
		380	14	3.6	2.1	0.17
Q (Ta_2O_5)	6	300	6.8	0.40	0.0	0.04
		380	33	16	5.3	0.85
R (Ta_2O_5)	12	300	9.0	2.6	0.0	1.2
		380	30	16	5.5	1.7

[a] Number represents pH of reaction media, *S* implies a surfactant was used during synthesis.

Table 6
Temperatures at which 30, 50 and 90% conversion of toluene is achieved for various palladium loaded catalytic systems.

Catalyst	Conditions[a]	T_{30} (°C)	T_{50} (°C)	T_{90} (°C)
Pd/G (Nb_2O_5)	2, *S*	201	213	243
Pd/H (Nb_2O_5)	6, *S*	211	224	280
Pd/I (Nb_2O_5)	12, *S*	215	219	229
Pd/J (Nb_2O_5)	2	203	221	285
Pd/K (Nb_2O_5)	6	205	217	261
Pd/L (Nb_2O_5)	12	230	237	244
Pd/M (Ta_2O_5)	2, *S*	207	214	233
Pd/N (Ta_2O_5)	6, *S*	205	211	222
Pd/O (Ta_2O_5)	12, *S*	231	235	246
Pd/P (Ta_2O_5)	2	221	227	281
Pd/Q (Ta_2O_5)	6	194	207	260
Pd/R (Ta_2O_5)	12	210	212	220

[a] Number represents pH of reaction media, *S* implies a surfactant was used during synthesis.

little influence on the chemical composition of the support between group V_b elements. Whilst these curves are comparable to the as-synthesised materials it is noted that their low temperature activity is generally inferior to that of the hierarchically porous supports (cf. activities at 200 °C).

In this study it was shown how niobium doping had more influence on Pt supported catalysts than Pd supported catalysts, however the results from the present study highlight that Nb_2O_5 can increase low temperature activities with improved $T_{30\%}$ values for Pd/Nb_2O_5 than for Pd/1 and 3% Nb-doped titania (in all bar one case, 15–30 °C lower) suggesting that the promoting effect of niobium can be influenced by its bonding arrangement and local environment.

3.5. Surface acidity by NH_3-TPD

Based on the catalytic results one can see that the supports synthesised at pH 6 were the most active. To better understand their catalytic behaviour, these supports (H, K, N and Q) were analysed by NH_3-TPD to determine the density of acid sites on the supports.

In Fig. 7 two maxima are clearly observed in each curve. The low temperature peak at around 200 °C is associated with the desorption of NH_3 from weak-medium acid sites whereas the high temperature peak at around 375 °C is representative of stronger acid sites on a support. The contribution arising from the strong acid sites to the overall acidity is much more pronounced for the Ta_2O_5 supports. The total number of acid sites per gram in the Nb_2O_5 samples, H and K, is greater than for their counterpart Ta_2O_5 sample, N and Q, respectively (Table 9). When comparing the % conversion of toluene it can be seen that Nb_2O_5 samples are more active than Ta_2O_5 with a conversion of K > H ≈ Q > N for 300 °C and K > H > Q ≈ N for 380 °C. Thus in correlating the datasets it could be suggested that toluene oxidation is facilitated by the highest number of acid sites per gram and that the presence of strong acid sites makes toluene oxidation more difficult as the adsorption of toluene molecules on these strong acid sites could lead to difficulties in their activation.

Interestingly the total number of acid sites per gram in the samples synthesised in the presence of a micellar solution (H and N) are greater than for the samples synthesised in distilled water alone irrespective of chemical composition (Nb_2O_5 and Ta_2O_5). This suggests that the non-ionic surfactant also plays a role in the surface chemistry of the hierarchically porous materials. Furthermore it can be seen that although both Nb_2O_5 samples had more acid sites per gram, they had a lower acid density (specific acidity) than their Ta_2O_5 counterparts (H vs N and K vs Q) owing to the differences in the specific surfaces, which were lower for both Ta_2O_5 samples than for either Nb_2O_5 (see Tables 2 and 3).

In contrast to V^{5+}, bulk oxides of Nb^{5+} and Ta^{5+} rarely contain MO_4 units, preferring MO_5/MO_6 co-ordinations owing to their large size [32]. The structure of niobium oxide compounds is often based on the octahedrally co-ordinated NbO_6 structure, where the distortion within the lattice depends on whether the polyhedra are corner or edge shared [7]. It has been shown that $Nb_2O_5 \cdot nH_2O$ can have a few highly distorted NbO_6 sites. Such octahedra possess Nb=O bonds, which are associated with Lewis acid sites, whereas when the distortion is slight only Nb—O bonds are present which are associated with Brønsted acid sites [33].

In fact both $Nb_2O_5 \cdot nH_2O$ and $Ta_2O_5 \cdot nH_2O$ are highly acidic, however this acidity decreases with increasing temperature, with

Table 7
Catalytic activity and selectivity in the oxidation of toluene over palladium loaded hierarchically porous supports.

Catalyst	Conditions[a]	Pd content (wt%)	T (°C)	Activity[b] (h^{-1})	Toluene conversion (%)	Selectivity (%)		
						CO_2	CO	Benzene
Pd/G (Nb_2O_5)	2, *S*	0.415	200	29	39	28	0.0	0.31
			250	52	97	92	0.0	0.14
Pd/H (Nb_2O_5)	6, *S*	0.342	200	26	9.6	4.1	0.0	0.22
			250	61	74	72	0.0	0.15
Pd/I (Nb_2O_5)	12, *S*	0.387	200	18	18	9.4	0.0	0.23
			250	55	99	97	0.0	0.15
Pd/J (Nb_2O_5)	2	0.450	200	24	28	21	0.0	0.30
			250	42	75	72	0.0	0.23
Pd/K (Nb_2O_5)	6	0.203	200	41	40	21	0.0	0.72
			250	97	93	81	0.0	0.24
Pd/L (Nb_2O_5)	12	0.258	200	24	9.2	4.1	0.0	0.07
			250	81	99	93	0.0	0.18
Pd/M (Ta_2O_5)	2, *S*	0.444	200	14	21	18	0.0	0.25
			250	44	98	93	0.0	0.16
Pd/N (Ta_2O_5)	6, *S*	0.248	200	24	30	34	0.0	0.11
			250	82	99.7	98	0.0	0.07
Pd/O (Ta_2O_5)	12, *S*	0.417	200	9.2	14	6.2	0.0	0.36
			250	50	97	95	0.0	0.74
Pd/P (Ta_2O_5)	2	0.426	200	10	19	5.5	0.0	0.08
			250	49	92	86	0.0	0.88
Pd/Q (Ta_2O_5)	6	0.270	200	39	41	30	0.0	0.19
			250	69	89	83	0.0	0.09
Pd/R (Ta_2O_5)	12	0.345	200	5.6	5.9	1.3	0.0	0.00
			250	63	99	98	0.0	0.08

[a] Number represents pH of reaction media, *S* implies a surfactant was used during synthesis.
[b] Calculated in terms of mol toluene reacted over mol of Pd per hour.

Table 8
Catalytic data in the oxidation of toluene over palladium loaded commercial Nb_2O_5 and Ta_2O_5 oxides.

Control	T_{30} (°C)	T_{50} (°C)	T_{90} (°C)	Pd content (wt%)	T (°C)	Activity[a] (h^{-1})	Toluene conversion (%)	Selectivity (ppm)	
								CO	Benzene
Nb_2O_5	>400	>400	>400	–	300	–	0.52	–	0
					380	–	7.2	–	0
Pd/Nb_2O_5	204	210	215	0.39	200	13	19	0	18.5
					250	67	99.7	0	0
Ta_2O_5	>400	>400	>400	–	300	–	0.01	–	0
					380	–	0.95	–	0
Pd/Ta_2O_5	205	209	215	0.31	200	11	14	0	4.4
					250	84	99.6	0	8

[a] Calculated in terms of mol toluene reacted over mol of Pd per hour.

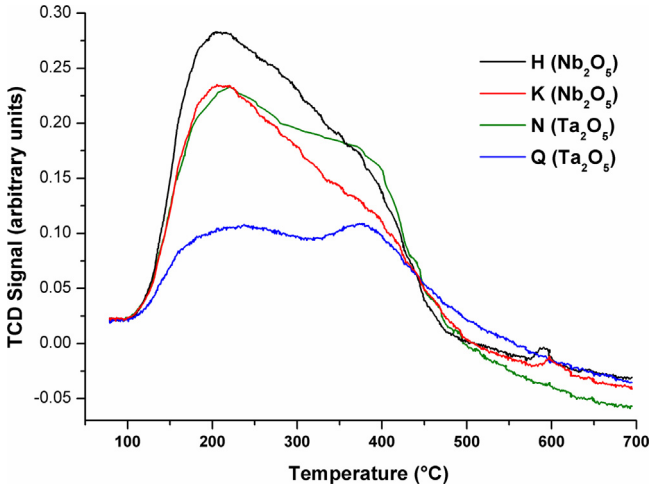

Fig. 7. TPD curves for the desorption of NH_3 over samples H, K, N and Q.

$Ta_2O_5{\cdot}nH_2O$ retaining more acidity at higher temperatures than $Nb_2O_5{\cdot}nH_2O$. In this work, the calcination temperature is kept low (400 °C) to prevent a wide scale collapse of the macropores, thus the structures remain quasi-amorphous and potentially some hydrated oxide remains thus imparting additional acidity to the structures.

Table 9
Quantification of acid sites by NH_3-TPD.

Sample	No. acid sites ($\mu mol\ g^{-1}$)	Acid density ($\mu mol\ m^{-2}$)
H (Nb_2O_5)	558	1.57
K (Nb_2O_5)	348	1.53
N (Ta_2O_5)	467	2.94
Q (Ta_2O_5)	144	2.53

4. Conclusion

This study has shown how the pH of the reactant medium is crucial in determining the textural properties of the oxide product and how the use of a micellar solution can impart additional porosity within the product, thereby increasing its surface area. Furthermore it can be seen that whilst niobium and tantalum are considered twin elements owing to their similar properties and the fact they occur together in nature, the results herein show how the hydrolysis of niobium ethoxide yields higher surface area oxides under acidic pH whereas for tantalum ethoxide the opposite is true. Here an alkaline pH yields the higher surface area products.

Catalytic testing reveals how group V_b metal oxides with multimodal porosities show great potential as supports for noble metal nanoparticles as these support materials alone can influence total oxidation processes. It has been supposed that improved surface areas and a more adept porous network that can aid matter transport through the catalytic system are beneficial to the overall process. However, the results have also shown that the initial pH of the reaction media used in the preparation of hierarchically porous oxides can influence the activity of the Pd/support system, most probably due to surface modifications such as acid site density which could alter support-metal interactions or the availability of oxygen at the VOC-catalyst interface or lead to an increase in adsorption of the VOC molecule on the catalyst surface rendering activation more difficult.

As the precursors of these materials are economically less interesting than cheaper silica or aluminosilicate based catalysts, it would be of interest to investigate whether smaller amounts of a noble metal-group V_b oxide system highly dispersed over a much cheaper bulk material would yield similar enhancements to the catalytic process. Although the mobility of both Nb_2O_5 and Ta_2O_5 is much lower than V_2O_5 owing to an increase in the temperature at which surface atoms begin to diffuse, the so called Tammann temperature (620 and 800 °C for Nb_2O_5 and Ta_2O_5, respectively, versus 209 °C for V_2O_5), when working at temperatures beyond the Tammann temperature or when employing such catalysts in the liquid phase there is a risk that V^{5+} species are liberated from the surface of the support leading to a degeneration in the catalytic system.

Acknowledgements

This work was supported through a European Union project, REDUGAZ, funded by the Interreg IV France-Wallonie-Flandre (FW 4.1.5) programme and via an IRENI research grant provided by Région Nord Pas de Calais, the French State and ERDF and the CNRS. The authors want to warmly thank Mr. Olivier Gardoll from UCCS for his technical help on NH_3-TPD experiments.

Appendix A. Supplementary data

Supplementary material related to this article can be found, in the online version, at http://dx.doi.org/10.1016/j.apcatb.2014.06.056.

References

[1] A. Brückner, Catal. Rev. 45 (2003) 97–150.
[2] L. Lloyd in, M.V. Twigg, M.S. Spencer, Handbook of Industrial Catalysts, in: Fundamental and Applied Catalysis Series Eds., Springer, New York, NY, 2011, pp. 34–36.
[3] H. Bosch, F.J.J.G. Janssen, F.M.G. Van den Kerkhof, J. Oldenziel, J.G. Van Ommen, J.R.H. Ross, Appl. Catal. 25 (1986) 239–248.
[4] M. Vassileva, A. Andreev, S. Dancheva, Appl. Catal. 69 (1991) 221–234.
[5] (a) I.E. Wachs, B.M. Weckhuysen, Appl. Catal., A: Gen. 157 (1997) 67–90; (b) A. Khodakov, B. Olthof, A.T. Bell, E. Iglesia, J. Catal. 181 (1999) 205–216; (c) Y.-M. Liu, Y. Cao, N. Yi, W.-L. Feng, W.-L. Dai, S.R. Yan, H.-Y. He, K.N. Fan, J. Catal. 224 (2004) 417–428.
[6] B.M. Weckhuysen, D.E. Keller, Catal. Today 78 (2003) 25–46.
[7] I. Nowak, M. Ziolek, Chem. Rev. 99 (1999) 3603–3624.
[8] (a) R. Brown, C. Kemball, J. Chem. Soc., Faraday Trans. 92 (1996) 281–288; (b) T. Uchijima, Catal. Today 28 (1996) 105–117; (c) K. Kunimori, H. Shindo, D. Nishio, T. Sugiyama, T. Uchijima, Bull. Chem. Soc. Jpn. 67 (1994) 2567–2570; (d) R. Rodrigues, N. Isoda, M. Gonçalves, F.C.A. Figueiredo, D. Mandelli, W.A. Carvalho, Chem. Eng. J. 198–199 (2012) 457–467; (e) D.A.G. Aranda, A.L.D. Ramos, F.B. Passos, M. Schmal, Catal. Today 28 (1996) 119–125.
[9] T. Ushikubo, Catal. Today 57 (2000) 331–338.
[10] T. Iizuka, K. Ogasawara, K. Tanabe, Bull. Chem. Soc. Jpn. 56 (1983) 2927–2931.
[11] M. Inês de Sairre, E.S. Bronze-Uhle, P.M. Donate, Tetrahedron Lett. 46 (2005) 2705–2708.
[12] K. Tanabe, Catal. Today 8 (1998) 1–11.
[13] T. Ushikubo, Catal. Today 78 (2003) 79–84.
[14] Y. Chen, J.L.G. Fierro, T. Tanaka, I.E. Wachs, J. Phys. Chem. B 107 (2003) 5243–5250.
[15] M.A. Aegerter, Sol. Energy Mater. Sol. Cells 68 (2001) 401–422.
[16] K. Nakajima, T. Fukui, H. Kato, M. Kitano, J.N. Kondo, S. Hayashi, M. Hara, Chem. Mater. 22 (2010) 3332–3339.
[17] Y. Takahara, J.N. Kondo, T. Takata, D. Lu, K. Domen, Chem. Mater. 13 (2001) 1194–1199.
[18] T. Sreethawong, S. Ngamsinlapasathian, Y. Suzuki, S. Yoshikawa, J. Mol. Catal. A: Chem. 235 (2005) 1–11.
[19] D.M. Antonelli, J.Y. Ying, Angew. Chem. Int. Ed. 35 (1996) 426–430.
[20] D.M. Antonelli, J.Y. Ying, Chem. Mater. 8 (1996) 874–881.
[21] (a) A. Collins, D. Carriazo, S.A. Davis, S. Mann, Chem. Commun. (2004) 568–569; (b) A. Vantomme, A. Léonard, Z.-Y. Yuan, B.-L. Su, Colloids Surf., A: Physicochem. Eng. Aspects 300 (2007) 70–78; (c) J. Rooke, T. Barakat, S. Siffert, B.-L. Su, Catal. Today 192 (2012) 183–188.
[22] (a) A. Léonard, B.-L. Su, Chem. Commun. (14) (2004) 1674–|1675; (b) A. Vantomme, B.-L. Su, Stud. Surf. Sci. Catal. 165 (2007) 235–238; (c) Y. Li, X.-Y. Yang, G. Tian, A. Vantomme, J. Yu, G. Van Tendeloo, B.L. Su, Chem. Mater. 22 (2010) 3251–3258.
[23] J.L. Blin, A. Léonard, Z.-Y. Yuan, L. Gigot, A. Vantomme, A.K. Cheetham, B.-L. Su, Angew. Chem. Int. Ed. 42 (2003) 2872–2875.
[24] H.L. Tidahy, S. Siffert, J.-F. Lamonier, E.A. Zhilinskaya, A. Aboukaïs, Z.-Y. Yuan, A. Vantomme, B.-L. Su, X. Canet, G. de Weireld, M. Frère, T.B. N'guyen, J.-M. Giraudon, G. Leclercq, Appl. Catal., A: Gen. 310 (2006) 61–69.
[25] L.-H. Chen, X.-Y. Li, G. Tian, Y. Li, J. Rooke, G.-S. Zhu, S.-L. Qiu, X.-Y. Yang, B.-L. Su, Angew. Chem. Int. Ed. 50 (2011) 11156–11161.
[26] X.-Y. Li, L.-H. Chen, Y. Li, J.C. Rooke, C. Wang, Y. Lu, A. Krief, X.-Y. Yang, B.-L. Su, J. Colloid Interface Sci. 368 (2012) 128–138.
[27] M. Hosseini, S. SIffert, R. Cousin, A. Aboukaïs, Z. Hadj-Sadok, B.L. Su, C. R. Chimie 12 (2009) 654–659.
[28] D.R. Lide (Ed.), CRC Handbook of Chemistry and Physics, 85th ed., CRC Press, Boca Raton, FL, 2004, pp. 4–93.
[29] F. Rouquerol, J. Rouquerol, K. Sing, Adsorption by Powders and Porous Solids: Principles, Methodology and Applications, Academic Press, London, 1994, pp. 204–205.
[30] J.D. Wright, N.A.J.M. Sommerdijk, Sol Gel Materials: Chemistry and Applications, CRC Press, Boca Raton, FL, 2000, pp. 53–67.
[31] J.C. Rooke, T. Barakat, M. Franco Finol, P. Billemont, G. De Weireld, Y. Li, R. Cousin, J.M. Giraudon, S. Siffert, J.-F. Lamonier, B.-L. Su, Appl. Catal., B: Environ. 142–143 (2013) 149–160.
[32] I.E. Wachs, Y. Chen, J.-M. Jehng, L.E. briand, T. Tanaka, Catal. Today 78 (2003) 13–24.
[33] S.M. Maurer, E.I. Ko, J. Catal. 135 (1992) 125–134.